CellPress

Structure
Article

Crystal Structure of the Rab9A-RUTBC2 RBD Complex Reveals the Molecular Basis for the Binding Specificity of Rab9A with RUTBC2

Zhe Zhang,[1,2] Shanshan Wang,[1,2] Tong Shen,[1] Jiangye Chen,[1] and Jianping Ding[1,*]
[1]State Key Laboratory of Molecular Biology, Institute of Biochemistry and Cell Biology, Shanghai Institutes for Biological Sciences, Chinese Academy of Sciences, 320 Yue-Yang Road, Shanghai 200031, China
[2]Co-first author
*Correspondence: jpding@sibcb.ac.cn
http://dx.doi.org/10.1016/j.str.2014.08.005

SUMMARY

Rab9 plays a vital role in regulating the transport of mannose 6-phosphate receptors from late endosomes to the *trans*-Golgi network through interactions with various effectors. Here, we report the crystal structure of GTP-bound Rab9A in complex with the Rab-binding domain (RBD) of the effector RUTBC2. RUTBC2 RBD assumes a pleckstrin homology domain fold that uses a binding site consisting of mainly β1 and the η1 insertion to interact with the switch and interswitch regions of Rab9A. The C-terminal hypervariable region of Rab9A is disordered and thus not required for RUTBC2 binding. The conformational plasticity of the switch and interswitch regions of Rab9A primarily determines the specificity for RUTBC2. Our biochemical and biological data confirm these findings and further show that Rab9B can bind to RUTBC2 probably in a similar manner as Rab9A. These results together reveal the molecular basis for the binding specificity of Rab9A with RUTBC2.

INTRODUCTION

Rab GTPases comprise ~70 members and constitute the largest family of small GTPases (Barr and Lambright, 2010; Zerial and McBride, 2001). Rabs localize to distinct organelle membranes and function together with their effectors to play central roles in regulating the vesicle-mediated transport including vesicle budding, transport, tethering, and fusion in eukaryotic organisms (Bonifacino and Glick, 2004; Grosshans et al., 2006; Stenmark, 2009). Like other small GTPases, Rabs cycle between two states, the GTP-bound active state and the GDP-bound inactive state, and the conversions are assisted by guanine exchange factors (GEFs) and GTPase-activating proteins (GAPs). The active Rabs can bind a variety of effectors that can recruit motor proteins or serve as cargo adaptors and tethering factors to facilitate membrane trafficking.

Different Rabs can bind their specific effectors and then execute distinct functions in certain types or different steps of membrane trafficking (Barr and Lambright, 2010). Rabs commonly use the switch and interswitch regions to bind the effectors, such as in the Rab4/Rab22-Rabenosyn-5 (Eathiraj et al., 2005), Rab5-Rabaptin-5 (Zhu et al., 2004), Rab6-Rab6IP1 (Recacha et al., 2009), and Rab11-FIP2/FIP3 (Eathiraj et al., 2006; Jagoe et al., 2006; Shiba et al., 2006) complexes. This binding mode is mediated predominantly by a hydrophobic surface formed by the switch and interswitch regions including a hydrophobic triad of three conserved aromatic residues and a hydrophobic patch formed by three variable hydrophobic residues (Itzen and Goody, 2011; Merithew et al., 2001). In some cases, like in the Rab3-Rabphilin-3A (Ostermeier and Brunger, 1999), Rab7-RILP (Wu et al., 2005), and Rab27-Slp2-a/Slac2-a (Chavas et al., 2008; Kukimoto-Niino et al., 2008) complexes, in addition to the switch and interswitch regions, the so-called complementarity-determining regions (CDRs), which comprise the N and C termini and the α3–β5 loop and exhibit high sequence variation (Ostermeier and Brunger, 1999; Pereira-Leal and Seabra, 2000), are also involved in determining the binding specificity of Rabs for the effectors. Although the effectors have unrelated sequences and structural folds, their binding with Rabs can be divided into all-α-helical, mixed α-helical, β-β zipping, and bivalent modes (Khan and Ménétrey, 2013).

Rab9 is predominantly bound to late endosome membranes and is required for the transport of mannose 6-phosphate receptors (MPRs) from late endosomes to the *trans*-Golgi network (TGN) (Barbero et al., 2002; Lombardi et al., 1993). In addition, Rab9 can function in lysosome biogenesis and late endosome morphology (Ganley et al., 2004; Riederer et al., 1994). It can also act as a cellular target for some pathogens, such as HIV and *Salmonella*, and plays an important role in the pathogenic infection (McGourty et al., 2012; Murray et al., 2005). So far, several Rab9 effectors have been identified including p40, Tip47, GCC185, and RhoBTB3, all of which are involved in the recycling of MPRs. Tip47 and p40 are localized to the late endosome membranes and are involved in the cargo sorting of MPRs to the Rab9-bound late endosomal recycling vesicles (Carroll et al., 2001; Díaz et al., 1997; Hanna et al., 2002). GCC185 and RhoBTB3 are present on the TGN and function in the membrane fusion of the Rab9-bound vesicles and the TGN (Espinosa et al., 2009; Reddy et al., 2006). Moreover, HPS1-HPS4 of the BLOC-3 complex is shown to be a Rab9 effector, and thus Rab9 may regulate BLOC-3 function in the biogenesis of lysosome-related organelles (Kloer et al., 2010).

 ©2014 Elsevier Ltd All rights reserved

Rab9 has two isoforms, namely Rab9A and Rab9B. Recently, two Rab9A effectors, namely RUTBC1 and RUTBC2 (also called SGSM2 and SGSM1), were identified, which are conserved in many eukaryotic organisms (Nottingham et al., 2011, 2012). Human RUTBC1 is expressed ubiquitously in various tissues and RUTBC2 mainly in brain, heart, and testis, whereas mouse RUTBC1 and RUTBC2 are expressed in the neurons of central nervous system (Yang et al., 2007). RUTBC1 and RUTBC2 contain an N-terminal RPIP8/Unc-14/NESCA (RUN) domain and a C-terminal Tre-2/Bub2/Cdc16 (TBC) domain. RUN domain usually functions as protein-protein interaction domain and can act as effectors of some Rap and Rab GTPases (Callebaut et al., 2001), whereas TBC domain can display GAP activity toward some Rabs (Fukuda, 2011). The TBC domains of RUTBC1 and RUTBC2 exhibit GAP activity toward Rab32/Rab33B and Rab34/Rab36, respectively (Nottingham et al., 2011, 2012), but the exact function(s) of the RUN domains of RUTBC1 and RUTBC2 are yet unknown. The intermediate region between the RUN and TBC domains contains the binding site for both Rab9A and Rap (Nottingham et al., 2011, 2012; Yang et al., 2007).

The crystal structures of Rab9 bound with GDP or GppNHp (5′-guanylyl imidodiphosphate, a nonhydrolyzable GTP analog) have been determined previously and show a classical nucleotide binding fold similar to other small GTPases (Chen et al., 2004; Eathiraj et al., 2005; Wittmann and Rudolph, 2004). So far, although many Rab9 effectors have been identified, no structural information about any Rab9-effector complex has been reported, and thus the molecular basis for the binding specificity of Rab9 with its effectors is unknown. Here, we report the crystal structure of the GTP-bound Rab9A in complex with the Rab-binding domain (RBD) of RUTBC2. RUTBC2 RBD adopts a pleckstrin homology (PH) domain fold and uses a binding site consisting of mainly β1 and the η1 insertion via a "mixed α/β" mode to bind Rab9A. The C-terminal hypervariable region of Rab9A is disordered in this complex structure and thus is not required for RUTBC2 binding. The conformational plasticity of the switch and interswitch regions of Rab9A primarily determines the specificity for RUTBC2. Our biochemical and biological data confirm these findings and further show that Rab9B can also bind to RUTBC2 probably in a similar manner as Rab9A. These data together reveal the molecular basis for the binding specificity of Rab9A with RUTBC2.

RESULTS

Crystal Structure of the Rab9A-RUTBC2 RBD Complex

It was reported previously that the Rab-binding domain (RBD) of RUTBC1/RUTBC2 lies in the intermediate region (residues 188–450) between the RUN and TBC domains (Nottingham et al., 2011, 2012) (Figure 1A). To narrow down the exact binding domain of RUTBC2 required for Rab9A binding, we constructed a series of truncation forms of mouse RUTBC2 and tested their binding abilities with mouse Rab9A by GST pull-down assay. The results showed that a minimal fragment of RUTBC2 (residues 254–425) could form a stable complex with the GTP-bound constitutively active Rab9A Q66L mutant (residues 1–199). This complex could be purified in the presence of GTP and Mg^{2+} with high stability and homogeneity and be crystallized in space group $P2_12_12_1$. The crystal structure of the Rab9A-RUTBC2 RBD complex was solved at 2.30 Å resolution and the asymmetric unit contains one complex (Figures 1B and S1A; Table 1). Residues 6–177 of Rab9A are well defined and the C-terminal hypervariable region (residues 178–199) is disordered. The bound GTP and Mg^{2+} at the active site are also clearly defined. Residues 254–424 of RUTBC2 RBD are well defined except for the loop before the last β strand (residues 390–413).

The structure of RUTBC2 RBD is composed mainly of seven β strands forming two β sheets (β1–β4, and β5–β6 and β8, respectively) and an abutting α helix (α1) sandwiched by the β sheets. In addition, one short β strand (β7) and five 3_{10} helices (η1–η5) are scattered in the connecting loops (Figures 1B and S1B). A structural similarity search using the DALI server (Holm and Rosenström, 2010) reveals that the core structure of the RBD adopts a pleckstrin homology (PH) domain fold with the highest similarity to the GRAM domain of MTMR2 (a *Z* score of 9.3 and a root-mean-square deviation [rmsd] of 2.0 Å for 88 Cα atoms) (Begley et al., 2003) and Exo84 (a *Z* score of 8.7 and an rmsd of 2.4 Å for 86 Cα atoms) (Jin et al., 2005) (Figure 1C) despite of their very low sequence similarities (~12%). Nevertheless, there are great variations in both sequence and length of the loop regions that appear to supplement the β sandwich core to render diverse binding sites for protein partners (Figure S1C). For example, RUTBC2 RBD contains a relatively long insertion in the β3–β4 loop that forms three 3_{10} helices (η1–η3) and is involved in the interaction of Rab9A (see results later). It is also noteworthy that in RUTBC2 RBD, the region corresponding to β7 of the three-stranded β sheet in the canonical PH domains assumes a loop conformation, and instead, the C-terminal region forms an extra β strand (β8) to make the three-stranded β sheet with β5 and β6 (Figure 1C).

In the Rab9A-RUTBC2 RBD complex, the overall structure of the GTP-bound Rab9A is very similar to that of the GppNHp-bound Rab9A (an rmsd of 0.67 Å for 170 Cα atoms) (Eathiraj et al., 2005) as well as the GDP-bound Rab9A (an rmsd of 0.87 Å for 170 Cα atoms) (Chen et al., 2004) (Figure 1D). However, the switch and interswitch regions assume the active conformation similar to that in the GppNHp-bound Rab9A but different from that in the GDP-bound Rab9A. There are only a few residues in the switch regions exhibiting notable conformational differences from these in the GppNHp-bound Rab9A, including Phe37, Glu43, and Arg68 of Rab9A, which are all involved in either hydrophobic or hydrophilic interactions with RUTBC2 RBD (Figure 1D).

Interactions between Rab9A and RUTBC2 RBD

The interactions between Rab9A and RUTBC2 RBD involve switch I, switch II, and a small part of the interswitch region of Rab9A, and β1, β2, and η1 of RUTBC2 RBD (Figures 1B, 2A, and 2B). The CDRs of Rab9A including the C-terminal hypervariable region are not involved in the interactions (Figures 1B and 2C). At the interaction interface, Rab9A and RUTBC2 RBD show good complementarities in both geometrical and electrostatic properties (Figure 2D). The interaction interface buries a total solvent accessible surface area of 1,292 $Å^2$ and consists of two hydrophobic patches and a hydrophilic patch. At one

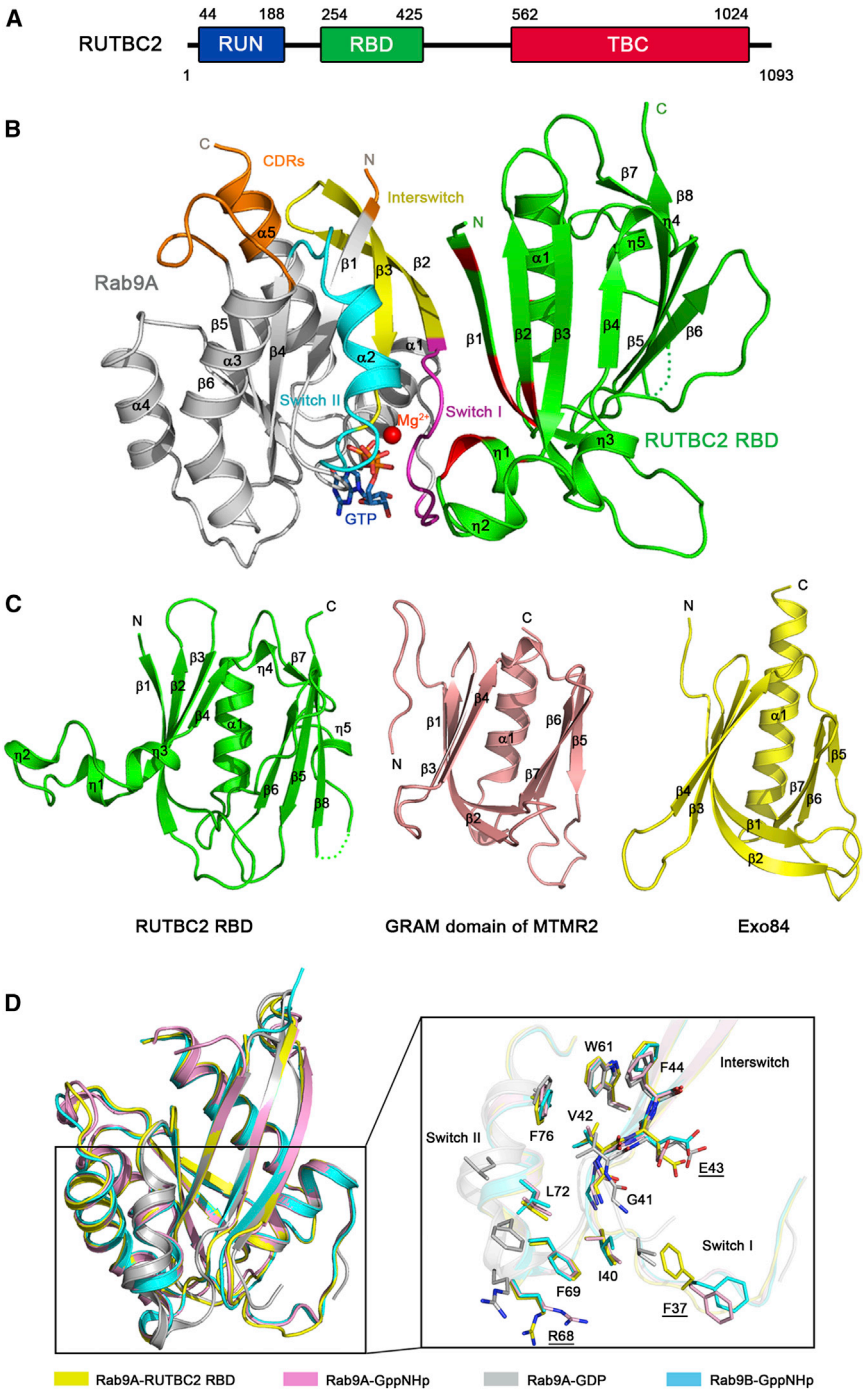

Figure 1. Crystal Structure of the Rab9A-RUTBC2 RBD Complex

(A) A schematic diagram showing the domain organizations of RUTBC2.

(B) A ribbon representation of the overall structure of the Rab9A-RUTBC2 RBD complex. The switch I, interswitch, switch II, and CDRs of Rab9A are colored in magenta, yellow, cyan, and orange, respectively, and the rest of Rab9A is colored in gray. The bound GTP and Mg^{2+} are shown with a stick model and a red sphere, respectively. RUTBC2 RBD is shown in green and the residues participating in interactions with Rab9A are highlighted in red. Rab9A and RUTBC2 RBD are labeled with secondary structures. The C-terminal hypervariable domain (residues 178–199) of Rab9A and the loop between η5 and β8 (residues 390–413) of RUTBC2 RBD are disordered. The disordered loop in RUTBC2 RBD is shown with a dotted line.

(C) Structural comparison of RUTBC2 RBD (green), the GRAM domain of MTMR2 (salmon, PDB code 1LW3) (Begley et al., 2003), and Exo84 (yellow, PDB code 1ZC3) (Jin et al., 2005). These PH domains are shown in similar orientations.

(D) Structural comparison of Rab9A/Rab9B in different nucleotide-bound forms. The GTP-bound Rab9A in the Rab9A-RUTBC2 RBD complex is colored in yellow, the GppNHp-bound Rab9A (PDB code 1YZL) (Eathiraj et al., 2005) in pink, the GDP-bound Rab9A (PDB code 1WMS) (Chen et al., 2004) in gray, and the GppNHp-bound Rab9B (PDB code 2OCB) in cyan. The zoom-in panel shows a detailed comparison of the switch and interswitch regions. The residues exhibiting notable conformational differences are underlined.

See also Figures S1, S5, and S6.

hydrophobic patch, the conserved hydrophobic triad (Phe44, Trp61, and Phe76) of Rab9A surround Leu256 in β1 of RUTBC2 RBD, making compact hydrophobic interactions (Figures 2A and 2B). At the other hydrophobic patch, Phe37 and Ile40 in switch I and Phe69 and Leu72 in switch II of Rab9A make extensive hydrophobic interactions with Asn262 in β1 and Asn294 and Met297 in η1 of RUTBC2 RBD (Figures 2A and 2B). In between the two hydrophobic patches, the conserved "IGVEF" motif of switch I forms a hydrophilic patch to interact with several polar residues of RUTBC2 RBD (Figures 2A and 2B). Specifically, the main-chain amino of Ile40 and the amino and carbonyl of Gly41 form three hydrogen bonds with the side chain of Asn261 in β1 of RUTBC2 RBD; the main-chain carbonyl of Val42 forms a hydrogen bond with the side chain of Tyr277 in β2 of RUTBC2 RBD; and the side chain of Glu43 forms a hydrogen bond with the side chain of Asn261 and a salt bridge with the side chain of Lys260 in β1 of RUTBC2 RBD. At the peripheral sides, the main-chain carbonyl of Phe44 in the interswitch and the side chain of Arg68 in switch II each form a hydrogen bond with the side chain of Gln361 in α1 and the main-chain carbonyl of Asn298 in η1 of RUTBC2 RBD, respectively.

Mutational Analyses of the Rab9A-RUTBC2 RBD Interaction

To verify the biological relevance of the Rab9A-RUTBC2 RBD complex in vitro, we first mutated the key residues of both Rab9A Q66L (residues 1–199) and RUTBC2 RBD (residues 254–425) at the interaction interface to Ala and tested their

 ©2014 Elsevier Ltd All rights reserved

Table 1. Summary of Diffraction Data and Structure Refinement Statistics

	Rab9A-RUTBC2 RBD
Diffraction Data	
Wavelength (Å)	0.9789
Space group	$P2_12_12_1$
Cell parameters	
a (Å)	52.8
b (Å)	60.0
c (Å)	127.8
$\alpha = \beta = \gamma$ (°)	90.0
Resolution (Å)	50.00–2.30 (2.38–2.30)[a]
Observed reflections	107,241
Unique reflections ($I/\sigma(I) > 0$)	18,655
Average redundancy	5.7 (6.0)
Average $I/\sigma(I)$	19.6 (4.7)
Completeness (%)	98.7 (100.0)
R_{merge} (%)[b]	7.9 (35.4)
Refinement and Structure Model	
Reflections ($Fo \geq 0\sigma(Fo)$)	
Working set	17,468
Test set	961
R_{work}/R_{free} (%)[c]	18.1/23.3
No. of atoms	2,696
Protein	2,559
GTP	32
Mg^{2+}	1
Water	104
Average B factor (Å^2)	
All atoms	56.3
Main-chain atoms	53.2
Side-chain atoms	60.4
GTP	33.6
Mg^{2+}	36.0
Water	51.7
Rmsd	
Bond lengths (Å)	0.009
Bond angles (°)	1.2
Ramachandran plot (%)	
Most favored	91.7
Allowed	7.9
Generously allowed	0.4

[a]Numbers in parentheses represent the highest resolution shell.
[b]$R_{merge} = \sum_{hkl}\sum_i|I_i(hkl)_i - \langle I(hkl)\rangle|/\sum_{hkl}\sum_i I_i(hkl)$.
[c]$R = \sum_{hkl}||F_o| - |F_c||/\sum_{hkl}|F_o|$.

effects on the Rab9A-RUTBC2 RBD interaction by both GST pull-down assay and isothermal titration calorimetry (ITC) analysis. Our biochemical results show that these mutations have no effects on the solubility and stability of the proteins (data not shown). In addition, our high-performance liquid chromatography (HPLC) analysis results show that the mutations of Rab9A do not affect the GTP binding (data not shown). However, our GST pull-down and ITC analysis results show that these mutations impair the Rab9A-RUTBC2 RBD interaction to varying degrees (Figures 3A, 3B, S2A, and S2B; Table 2). On the Rab9A side, mutations I40A, V42A, F44A, W61A, F69A, L72A, and F76A decrease the binding ability of Rab9A to RUTBC2 RBD by >50% as shown by the GST pull-down results and increase their dissociation constants (K_d) by 30- to 100-fold as shown by the ITC results, suggesting that these hydrophobic contacts play an important role in the interaction. Intriguingly, mutation F37A has insignificant effect on the interaction (Figures 3A, 3B, and S2A; Table 2), consistent with the observation that this residue is highly varied among different Rab GTPases and thus might play a less critical role in the binding of the effector (Figure 2C). Mutation of Gly41 to either Ala or Asp dramatically impairs the binding ability by >70% and consistently these mutants have no measurable K_d probably due to their potential steric conflicts with RUTBC2 RBD. Mutation E43A diminishes the binding ability to <15% and significantly increases the K_d by ~230-fold as this mutation disrupts the hydrogen-bonding and salt bridge interactions with RUTBC2 RBD in the hydrophilic core, suggesting that these hydrophilic interactions also play a critical role in the Rab9A-RUTBC2 RBD interaction. In contrast, the R68A mutant retains ~80% of the binding ability and the K_d is increased only by ~8-fold as this residue is located at one peripheral edge and its mutation does not affect the core interactions. On the RUTBC2 RBD side, mutations L256A, K260A, N261A, Y277A, N294A, and M297A severely abolish its binding with Rab9A and these mutants have either dramatically increased K_d (70- to 140-fold, L256A, K260A, and M297A) or no measurable K_d (N261A, Y277A, and N294A) as these residues participate in the extensive hydrophobic and hydrophilic interactions (Figures 3A, 3B, S2A, and S2B; Table 2). However, mutations of Asn262 (that has few hydrophobic contacts) and Gln361 (that forms a hydrogen bond with Phe44 of Rab9A at the other peripheral edge) to Ala have less significant effects on the Rab9A binding as shown by both GST pull-down results and ITC results. These results support the structural data very well.

To verify the functional role of the Rab9A-RUTBC2 interaction in vivo, we cotransfected the wild-type and several mutants of full-length Rab9A (WT, I40A, G41A, F44A, and I40A/G41D/F44A) and full-length RUTBC2 (WT, L256A, N261A, Y277A, and L256A/N261A/Y277A) into HeLa cells and analyzed the localization patterns of the two proteins (Figures 3C and S2C). In the cells cotransfected with the wild-type Rab9A and RUTBC2, most of Rab9A localize to the vesicle membranes with a relatively concentrated distribution pattern, and some of RUTBC2 are recruited to the Rab9A-positive membranes and colocalize well with Rab9A although most of RUTBC2 diffuse in the cytoplasm. However, in the cells cotransfected with either or both of the Rab9A and RUTBC2 mutants (either single mutation or triple mutation), RUTBC2 is diffusely distributed in the cytoplasm and cannot localize to the Rab9A-posivie vesicles as these mutations disrupt the Rab9A-RUTBC2 RBD interaction, consistent with our in vitro GST pull-down and ITC results. These functional analysis results together indicate that the Rab9A-RUTBC2 RBD interaction is biologically relevant and is essential for the membrane localization of RUTBC2.

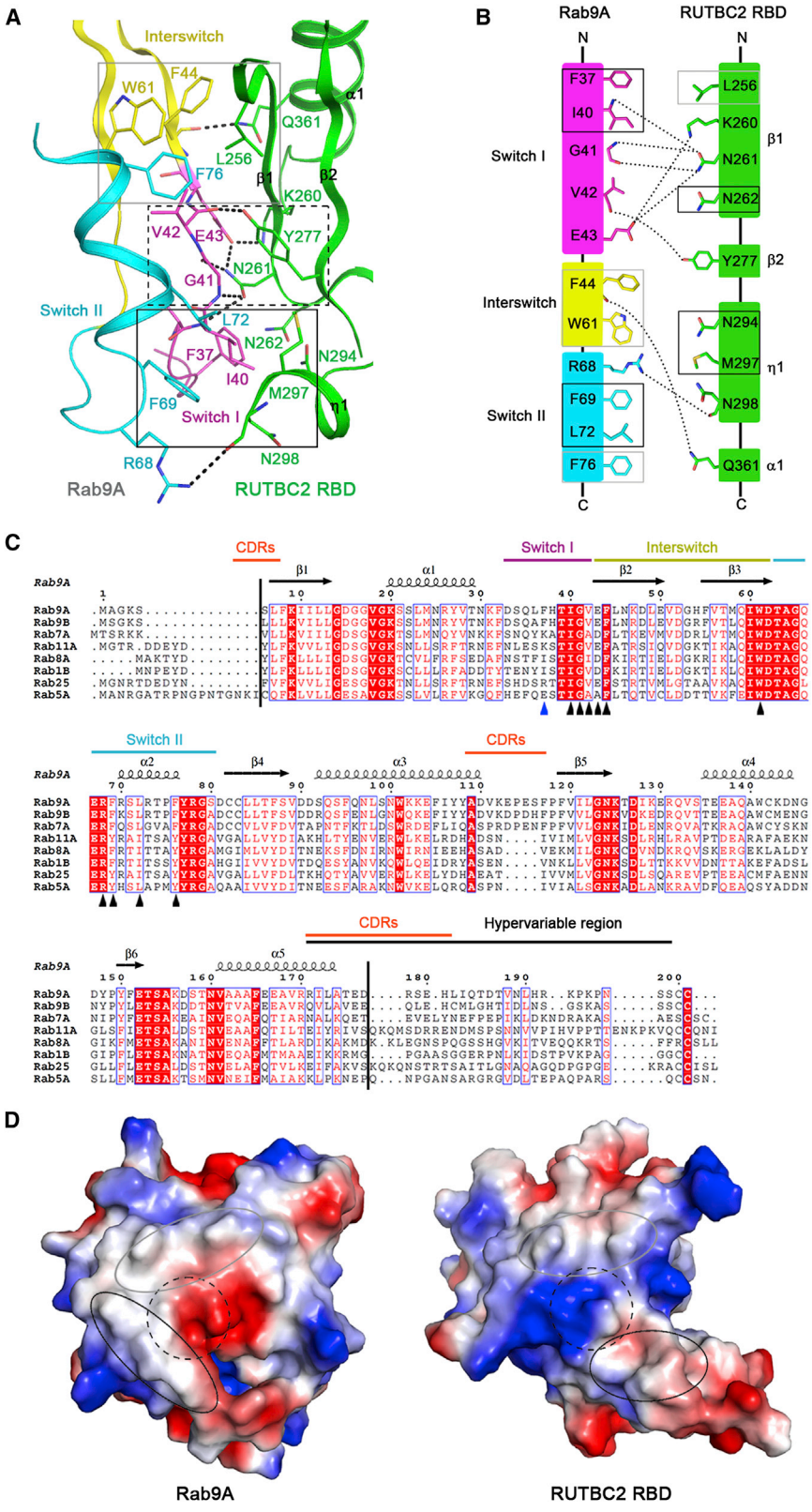

Figure 2. Interactions between Rab9A and RUTBC2 RBD

(A) A ribbon representation of the interaction interface between Rab9A and RUTBC2 RBD. The color scheme is the same as that in Figure 1B. The interacting residues are shown with side chains and the hydrophilic interactions are indicated with dotted lines. The interface can be divided into three patches including two hydrophobic patches (boxed by solid lines in gray and black, respectively) and a hydrophilic patch in between (boxed by dotted lines).

(B) A schematic diagram showing the interactions between Rab9A and RUTBC2 RBD. The color scheme is the same as that in (A). The interacting residues are shown with side chains. The hydrophilic interactions are indicated with dotted lines and the residues involved in two hydrophobic interaction surfaces are boxed by solid lines as that in (A).

(C) Sequence alignment of several representative Rab GTPases. The switch and interswitch regions, the CDRs, and the hypervariable region are indicated. The region observed in the Rab9A-RUTBC2 RBD structure is indicated using two horizontal bars. The residues involved in interactions with RUTBC2 RBD are indicated with triangles, with the conserved residues colored in black and the variable one in blue.

(D) Electrostatic surface representations of Rab9A and RUTBC2 RBD. The hydrophobic and hydrophilic patches at the interface are circled with solid and dotted lines, respectively. The surfaces of Rab9A and RUTBC2 RBD at the interaction interface show both geometrical and electrostatic complementarities.

 ©2014 Elsevier Ltd All rights reserved

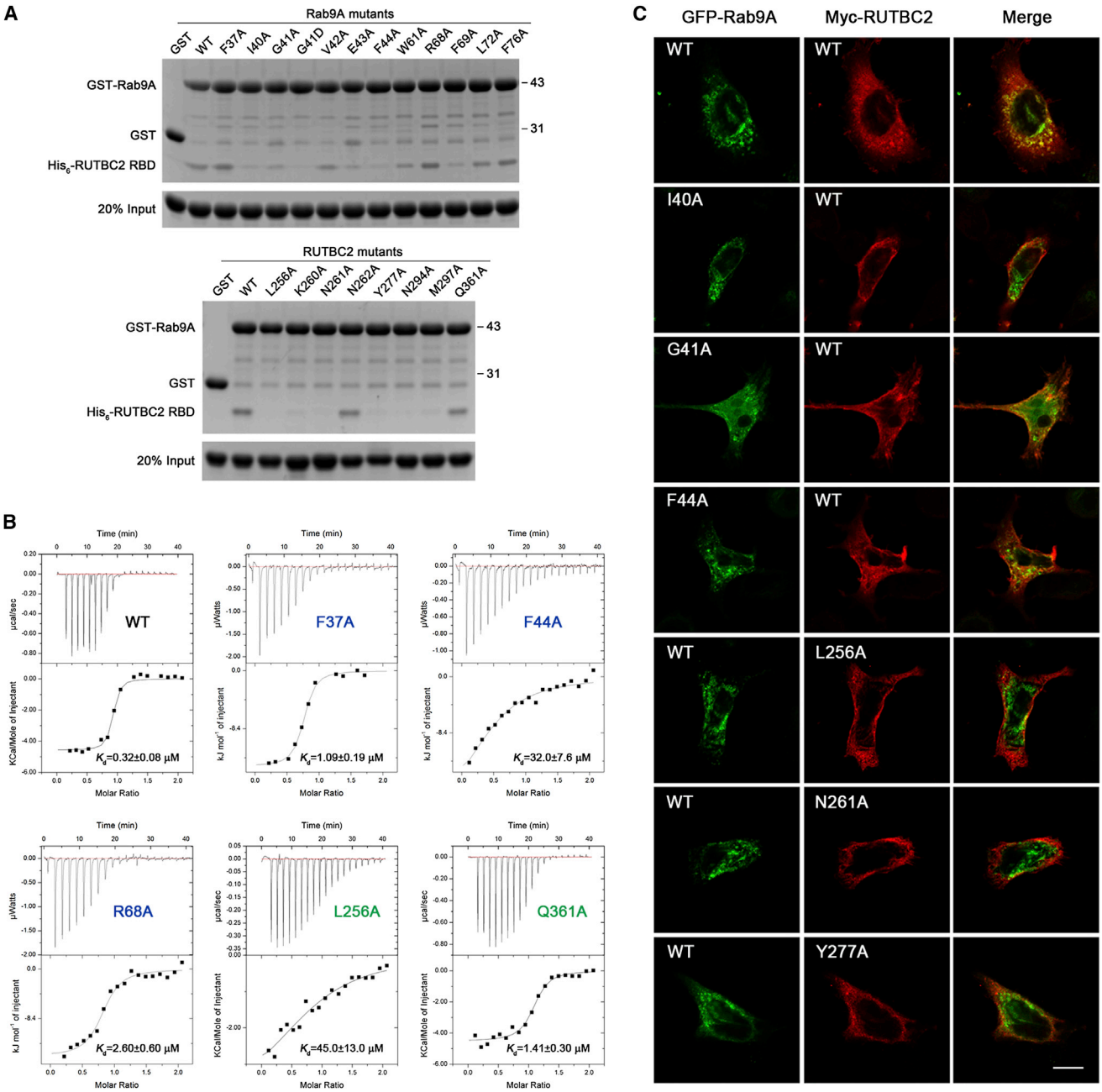

Figure 3. Mutational Analyses of the Rab9A-RUTBC2 RBD Interaction

(A) Upper panel: in vitro GST pull-down assays between the wild-type (Q66L) and mutant GST-Rab9A and the wild-type His_6-RUTBC2 RBD. Lower panel: in vitro GST pull-down assays between the wild-type (Q66L) GST-Rab9A and the wild-type and mutant His_6-RUTBC2 RBD. The gels were stained by Coomassie blue.
(B) Isothermal titration calorimetry (ITC) analyses of the binding affinities between the wild-type (Q66L) and mutant His_6-Rab9A and the wild-type and mutant His_6-RUTBC2 RBD. Rab9A mutants are labeled in blue and RUTBC2 RBD mutants in green. The dissociation constant (K_d) is indicated.
(C) Confocal fluorescence microscopy images of HeLa cells coexpressing GFP-Rab9A and Myc-RUTBC2 or their mutants. Scale bar represents 10 μm.
See also Figure S2.

Both Rab9A and Rab9B Can Bind to RUTBC2 and the Hypervariable Region Is Not Required for RUTBC2 Binding

It was shown previously that RUTBC1 and RUTBC2 can interact with both Rab9A and Rab9B based on the yeast two-hybrid screening analyses; however, they can only bind Rab9A based on the in vitro GST pull-down assays (Nottingham et al., 2011, 2012). As Rab9A and Rab9B are highly diverged in the C-terminal hypervariable region, Nottingham et al. (2011, 2012) suggested that RUTBC1 and RUTBC2 might recognize part of the hypervariable region of Rab9A to distinguish from Rab9B. In the Rab9A-RUTBC2 RBD structure, Rab9A interacts with

Table 2. ITC Measured Thermodynamic Parameters between Rab9A (Q66L) and RUTBC2 RBD in Both Wild-Type and Mutant Forms and the Parameters between Different Rab9 Variants and RUTBC2 RBD

	K_d (μM)	ΔH (kcal/mol)	TΔS (kcal/mol)	n Value
Rab9A Mutants				
WT	0.32 ± 0.08	−4.57 ± 0.10	4.29	0.88 ± 0.01
F37A	1.09 ± 0.19	−3.28 ± 0.07	4.71	0.73 ± 0.01
I40A	26.7 ± 5.4	−2.98 ± 0.52	3.16	0.41 ± 0.05
G41A	ND	ND	ND	ND
G41D	ND	ND	ND	ND
V42A	10.5 ± 3.6	−1.69 ± 0.24	4.99	0.68 ± 0.07
E43A	72.5 ± 16.5	−18.4 ± 4.7	−12.8	0.42 ± 0.10
F44A	32.0 ± 7.6	−5.21 ± 1.15	0.81	0.51 ± 0.09
W61A	30.8 ± 5.9	−7.66 ± 1.05	−1.61	0.61 ± 0.06
R68A	2.60 ± 0.60	−3.52 ± 0.15	3.98	0.80 ± 0.02
F76A	12.7 ± 2.3	−6.84 ± 0.42	−0.28	0.77 ± 0.03
RUTBC2 RBD Mutants				
WT	0.32 ± 0.08	−4.57 ± 0.10	4.29	0.88 ± 0.01
L256A	45.0 ± 13.0	−4.17 ± 0.94	1.76	0.89 ± 0.13
K260A	23.6 ± 9.5	−2.53 ± 0.52	3.79	1.10 ± 0.14
N261A	ND	ND	ND	ND
N262A	0.85 ± 0.23	−2.92 ± 0.08	5.37	1.13 ± 0.02
Y277A	ND	ND	ND	ND
N294A	ND	ND	ND	ND
M297A	25.4 ± 5.4	−4.46 ± 0.41	1.82	1.08 ± 0.06
Q361A	1.41 ± 0.30	−4.52 ± 0.11	3.46	1.06 ± 0.02
Rab9 Variants				
Rab9A	0.32 ± 0.08	−4.57 ± 0.10	4.29	0.88 ± 0.01
Rab9AΔC	0.39 ± 0.07	−4.86 ± 0.08	3.88	1.03 ± 0.01
Rab9B	0.33 ± 0.07	−5.49 ± 0.14	3.34	0.62 ± 0.01
Rab9BΔC	0.79 ± 0.18	−4.64 ± 0.11	3.70	0.73 ± 0.01
Rab9A-GDP	40.0 ± 8.3	−4.02 ± 0.59	1.98	0.83 ± 0.08
Rab9A 1-201	0.77 ± 0.10	−4.69 ± 0.05	3.67	0.93 ± 0.01

ND, not detected.
See also Figures S2 and S3.

RUTBC2 RBD only through the switch and interswitch regions, and the C-terminal hypervariable region is disordered and thus is not required for the binding of RUTBC2 RBD (Figure 1B). Sequence comparison shows that the residues of Rab9A involved in the interactions with RUTBC2 RBD are strictly conserved in Rab9B (Figure 2C). Structural comparison also shows that the switch and interswitch regions in the GppNHp-bound Rab9B assume almost identical conformations as those in the GppNHp-bound Rab9A and the Rab9A-RUTBC2 RBD complex (rmsd of <1.00 Å for ~50 Cα atoms in the switch and interswitch regions) (Figure 1D). These results suggest that the C-terminal hypervariable region of Rab9A is unlikely involved in the binding of RUTBC2 and Rab9B should be able to bind to RUTBC2 in a similar way as Rab9A.

To verify those results, we analyzed the binding abilities and affinities between RUTBC2 RBD and Rab9A/Rab9B with (Rab9A/Rab9B, residues 1–199) or without (Rab9AΔC/Rab9BΔC, residues 1–171) the hypervariable region using in vitro GST pull-down and ITC analyses. Our GST pull-down results show that RUTBC2 RBD can bind to Rab9A and Rab9B with similar binding ability, and the presence or deletion of the hypervariable region of Rab9A and Rab9B does not affect their binding with RUTBC2 RBD (Figure 4A). In addition, our results show that RUTBC1 RBD can also bind to Rab9A and Rab9B with similar binding ability and property as RUTBC2 RBD (Figure 4A), consistent with the high sequence conservation of the RBD of RUTBC1 and RUTBC2 (73% identity) (Figure S4A). Our ITC results show that the K_d values of RUTBC2 RBD with Rab9A and Rab9B are 0.32 ± 0.08 μM and 0.33 ± 0.07 μM, respectively, and the K_d values of RUTBC2 RBD with Rab9AΔC and Rab9BΔC are 0.39 ± 0.07 μM and 0.79 ± 0.18 μM, respectively, consistent with our GST pull-down results (Figure 4B). Moreover, to ensure that other regions of RUTBC2 do not affect its binding with Rab9A/Rab9B, we analyzed the binding abilities of the full-length RUTBC2 with Rab9A/Rab9B and Rab9AΔC/Rab9BΔC by GST pull-down assays. Our results show that the full-length RUTBC2 can bind to both Rab9A and Rab9B and deletion of the C-terminal hypervariable region of Rab9A/Rab9B has no significant effect on the binding (Figure S4B). Taking our structural and biochemical data together, we conclude that both Rab9A and Rab9B can bind to RUTBC2 and the C-terminal hypervariable region of Rab9A/Rab9B is not required for RUTBC2 binding. Intriguingly, the previous biochemical data showed that the hypervariable region of Rab9A/Rab9B is required for the binding of some effectors such as Tip47 and p40 (Aivazian et al., 2006). It is unclear whether Rab9A/Rab9B could bind to these effectors in different way(s) from that to RUTBC2. More thorough studies are needed to resolve this issue.

Binding Specificity of Rab9A with RUTBC2

Previous biochemical data showed that RUTBC1/RUTBC2 can bind to Rab9A/B but not other Rabs (Nottingham et al., 2011, 2012). Consistently, our ITC results also show that there is no detectable interaction between RUTBC2 RBD and several representative Rabs including the closely related Rab7A and the distantly related Rab3A and Rab5A. Rabs usually use the switch and interswitch regions to recognize and bind the effectors (Eathiraj et al., 2005, 2006; Jagoe et al., 2006; Recacha et al., 2009; Shiba et al., 2006; Zhu et al., 2004). In some Rab-effector complexes, the CDRs of Rabs are also involved in determining the binding specificity for the effectors (Chavas et al., 2008; Kukimoto-Niino et al., 2008; Ostermeier and Brunger, 1999; Wu et al., 2005). In the structure of the Rab9A-RUTBC2 RBD complex, the binding site of Rab9A for RUTBC2 RBD is only composed of residues of the switch and interswitch regions. The major structural determinants of Rab9A for binding RUTBC2 RBD consist of the hydrophobic triad of three strictly conserved aromatic residues (Phe44, Trp61, and Phe76) of the switch and interswitch regions, several less conserved hydrophobic residues of the switch I/II regions, and the conserved "IGVEF" motif of switch I (Figures 2A and 2B). Sequence alignment indicates that the residues of Rab9A involved in the interactions with RUTBC2 RBD are highly conserved among all Rabs (Figure 2C). An obvious question is why RUTBC2 RBD can specifically bind to Rab9A but not other Rabs.

 ©2014 Elsevier Ltd All rights reserved

Detailed structural comparisons of the Rab9A-RUTBC2 RBD complex with several representative Rab-effector complexes including the Rab3A-Rabphilin-3A complex, the Rab5A-Rabaptin-5 complex, and the Rab7A-RILP complex, reveal some subtle but important conformational differences in the switch and interswitch regions between Rab9A and the other Rabs even though their overall structures are very similar (Figure 5). First, the conserved "IGVEF" motif of switch I in Rab9A assumes an outward conformation compared with the other Rabs so that the side chain of Glu43 and the main-chain amino or/and carbonyl groups of Ile40, Gly41, and Val42 can form extensive hydrogen bonds with RUTBC2 RBD. Second, the N terminus of the β2 strand in the interswitch region of Rab9A is one residue shorter than that in the other Rabs and this shortening appears to provide some conformational flexibility for the "IGVEF" motif of switch I to interact with RUTBC2 RBD. Third, the α2 helix formed by switch II in Rab9A is positioned closer to the switch I and interswitch regions than that in the other Rabs and thus the switch and interswitch regions can form the specific hydrophobic patches to bind RUTBC2 RBD. These results lead us to suggest that like in some Rab-effector complexes (Eathiraj et al., 2005; Merithew et al., 2001), the conformational plasticity of the switch and interswitch regions of Rab9A is the major determinant for the binding specificity with RUTBC2. Nevertheless, it should be noted that the subtle sequence differences in and around the switch and interswitch regions might affect the conformations of these regions and thus could also contribute in part to the binding specificity of Rab9A with RUTBC2 RBD. As Rab9B can also bind to RUTBC2 and Rab9B and Rab9A are highly conserved in both sequence and structure, we predict that Rab9B may bind to RUTBC2 RBD in a similar manner as Rab9A. Additionally, as the sequences of the RBD of RUTBC1/RUTBC2 are also highly conserved among different species (>50% similarity) and most of the residues participating in the Rab9A binding are strictly conserved (Figure S4A), we also predict that RUTBC1 may bind to Rab9A/Rab9B in a similar manner as RUTBC2.

DISCUSSION

So far, many Rab9 effectors have been identified; however, no structure of any Rab9-effector complex has been reported. The crystal structure of the Rab9A-RUTBC2 RBD complex together with our biochemical data reveals the molecular basis for the binding specificity of Rab9A with RUTBC2. Specifically, we show that the C-terminal hypervariable region of Rab9A is not required for RUTBC2 binding and the conformational plasticity of the switch and interswitch regions of Rab9A primarily determines the specificity for RUTBC2. In addition, our structural and biochemical data suggest that Rab9A/Rab9B may bind to RUTBC1/RUTBC2 in a similar manner. These findings can help us understand the biological functions of the PH domain containing proteins and the binding specificity of Rab GTPases with their effectors.

RUTBC2 RBD assumes a PH domain fold and functions as the effector of Rab9. PH domain is one of the most common domains in human genome and many PH domain-containing proteins are involved in cellular signaling, cytoskeletal organization, transcription, DNA repair, membrane trafficking, and phospholipid medication (Lemmon, 2004, 2007; Scheffzek and Welti, 2012). Some PH domains can bind specifically to phosphoinositides (PIs) with high affinities to target cellular membranes. However, most of the PH domains bind to PIs with only low or no affinities and are not membrane targeted or confined to particular cellular compartments; they can serve as protein-protein interacting platforms to bind to a variety of proteins and to execute diverse functions. For examples, some PH domains can serve as effectors of small GTPases and some others can bind to GEFs of small GTPases to regulate the GEF activities (Scheffzek and Welti, 2012).

For those PH domains that can bind to PIs with high affinities and specificities, a positively charged surface groove composed mainly of several basic residues can specifically bind distinct PIs (Lemmon, 2004, 2007; Scheffzek and Welti, 2012). For instances, DAPP1 uses the surface groove between the β1-β2 loop and the β3-β4 loop to bind phosphatidylinositol-(3,4,5)-triphosphate (PI(3,4,5)P3) and PI(3,4)P2 (Ferguson et al., 2000); and β-spectrin uses another surface groove between the β1-β2 loop and the β5-β6 loop to bind PI(4,5)P2 (Hyvönen et al., 1995) (Figure 6). Sequence comparison shows that there are no basic residues in the corresponding regions of RUTBC2 RBD (Figure S1C), consistent with the surface electrostatic analysis result showing that there is no obvious positively charged surface groove on RUTBC2 RBD (Figure 6). Moreover, no detectable binding of RUTBC2 RBD with some common PIs was observed using a highly sensitive lipid-overlay blot (data not shown). These results indicate that RUTBC2 RBD may not bind to PIs.

Although PH domains can act as effectors of small GTPases, the Rab9A-RUTBC2 RBD complex is the first structure of a PH domain effector complexed with a Rab GTPase (Figure 1). Structural analyses of the available small GTPase-PH domain complexes show that PH domains can bind to small GTPases using distinct binding sites or surfaces (Figure S5). In some cases, such as the RalA-Exo84 complex (Jin et al., 2005), the Rac2-PLC-γ2 complex (Bunney et al., 2009), the RhoA-PRG complex (Chen et al., 2010), and the Arf1-ARHGAP21 complex (Ménétrey et al., 2007), the PH domains interact with small GTPases mainly through the β5-β7 sheet and the following α1 helix. In other cases, such as the Arf6-Grp1 complex (Malaby et al., 2013), the Ran-RanBD1 complex (Vetter et al., 1999), and the Rac1-PLC-β2 complex (Jezyk et al., 2006), the PH domains interact with small GTPases mainly via the β1-β4 sheet and the peripheral regions. In the Rab9A-RUTBC2 RBD complex, the binding site of RUTBC2 RBD for Rab9A involves mainly the β1 strand and the η1 insertion, which is similar to that of RanBD1 and PLC-β2 for their respective small GTPases (Figure S5). Nevertheless, Ran and Rac1 lay along the β2 strand of the PH domain, while Rab9A packs against the β1 strand of the PH domain. It is also noteworthy that based on the binding features of the effectors with Rab and Arf GTPases, the binding modes are divided into "all α-helical," "mixed α-helical, "β-β zipping," and "bivalent" modes (Khan and Ménétrey, 2013). However, the binding of RUTBC2 RBD with Rab9A involves mainly the β1 strand and the η1 insertion that is different from these observed in the other Rab-effector complexes, and thus we refer to this binding mode as a "mixed α/β" mode that also includes the Rab5-EEA1 complex (Mishra et al., 2010) (Figure S6).

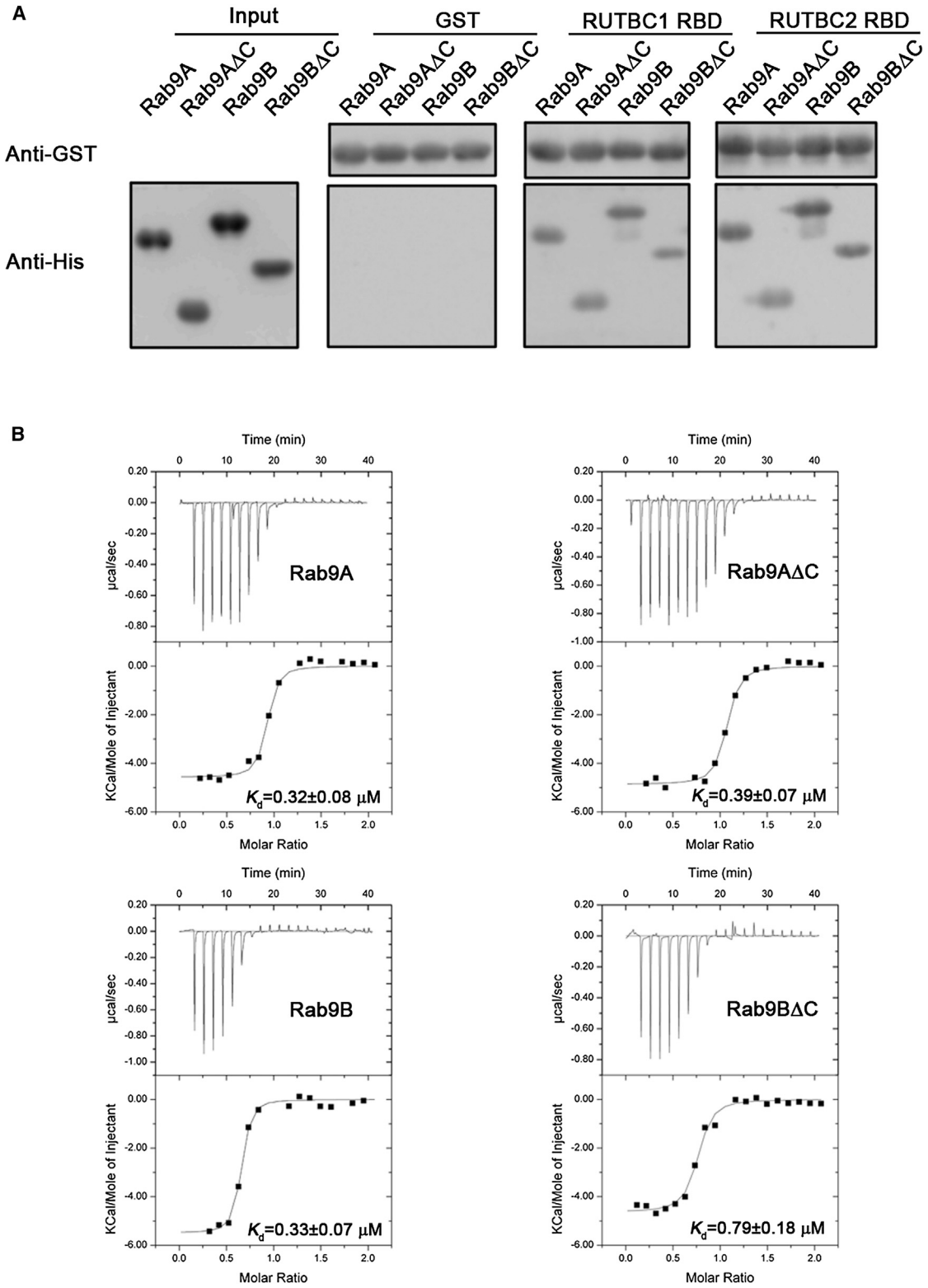

Figure 4. Analyses of the Interactions between Rab9A/Rab9B and RUTBC1/RUTBC2 RBD

(A) In vitro GST pull-down analyses of Rab9A/Rab9B with RUTBC1/RUTBC2 RBD. GST-RUTBC1/RUTBC2 RBD were preloaded onto the glutathione Sepharose beads and then incubated with His_6-Rab9A/Rab9B at 4°C for 2 hr. After washing three times with the lysis buffer, the beads were analyzed by western blotting

(legend continued on next page)

 ©2014 Elsevier Ltd All rights reserved

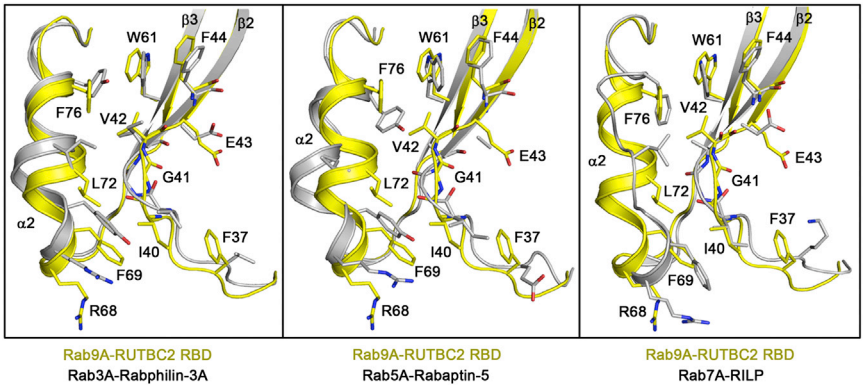

Figure 5. Structural Comparison of Representative Rabs in Complexes with their Effectors

Superpositions of Rab9A-RUTBC2 RBD with Rab3A-Rabphilin-3A (PDB code 1ZBD) (Ostermeier and Brunger, 1999), Rab5A-Rabaptin-5 (PDB code 1TU3) (Zhu et al., 2004), and Rab7A-RILP (PDB code 1YHN) (Wu et al., 2005) are shown in three panels, respectively, with Rab9A colored in yellow and the other Rabs in gray. The secondary structures are indicated.

The previous biochemical data showed that RUTBC2 can bind to Rap1/Rap2 using the so-called RAPID motif (residues 301-350) (Yang et al., 2007). This region also lies in the RBD of RUTBC2 and comprises mainly the β4-β6 strands (Figures 1B, 1C, and S4A). Structurally, the Rab9A and Rap binding sites have no overlap with each other, and thus RUTBC2 RBD could bind with Rab9A and Rap simultaneously. Given that Rab9 mainly controls the recycling of MPRs from late endosomes to the TGN (Pfeffer, 2009), while Rap mainly regulates the polarity and differentiation of neuronal cells, synaptic plasticity, cell-cell adhesion, and actin dynamics (Frische and Zwartkruis, 2010), and RUTBC1/RUTBC2 are expressed in many types of cells but are enriched in neuronal cells (Yang et al., 2007), the simultaneous binding of RUTBC1/RUTBC2 with Rab9 and Rap might mediate the crosstalk of the two signaling pathways in the development of neuronal cells. In addition, as the RUN domains could function as the effectors of some Rap and Rab GTPases (Callebaut et al., 2001), and the TBC domains of RUTBC1 and RUTBC2 have specific GAP activity for Rab32/Rab33B and Rab34/Rab36, respectively, all of which are involved in regulating the biogenesis of lysosome-related organelles (Nottingham et al., 2012), it is possible that RUTBC1/RUTBC2 might interact with these small GTPases to function synergistically in their sequential activation and inactivation to ensure the directionality of membrane transport events or bridge the crosstalk of different signaling pathways in broad cellular processes.

EXPERIMENTAL PROCEDURES

Cloning, Expression, and Purification of Proteins

Rab9A and RUTBC2 RBD were amplified by PCR from the cDNA library of mouse brain cells and cloned into the pET-22b plasmid (Novagen) that attaches a C-terminal His_6 tag and the pET-28a plasmid (Novagen) that attaches an N-terminal His_6 tag, respectively. The mutants were constructed using the QuikChange Site-Directed Mutagenesis kit (Strategene). The recombinant proteins were expressed in *Escherichia coli* BL21 (DE3) CodonPlus strain (Novagen). The transformed cells were grown at 37°C in LB medium containing 0.05 mg/ml ampicillin or kanamycin until OD_{600} reached 0.8 and then induced with 0.25 mM IPTG at 16°C for 24 hr. The harvested cells were lysed by sonication in a lysis buffer (20 mM Tris-HCl, pH 8.0, 1 mM $MgCl_2$, 150 mM NaCl, and 1 mM PMSF) and the cell lysates were centrifuged at 40,000 × *g* for 40 min. Rab9A and RUTBC2 RBD were purified separately by affinity chromatography using a Ni-NTA column (QIAGEN) in the lysis buffer. To get the Rab9A-RUTBC2 complex, the two proteins were mixed at 1:1 molar ratio in the lysis buffer and incubated with 1 mM GTP at 4°C overnight followed by gel filtration chromatography using a Superdex 200 16/60 column (GE Healthcare) in a storage buffer (20 mM Tris-HCl, pH 8.0, 1 mM $MgCl_2$, and 150 mM NaCl). The resultant sample was of >95% purity as evaluated by SDS-PAGE.

In Vitro GST Pull-Down Assay

Our biochemical studies show that the full-length Rab9A/Rab9B (residues 1–201) is partially dimerized in solution probably due to formation of a disulfide bond between the two cysteines at the C terminus (Figure S3). The partial dimerization of the full-length Rab9A/Rab9B could make their amounts bound to RUTBC2 RBD in more than 1:1 molar ratio in the GST pull-down assay although it does not affect the binding with RUTBC2 RBD. Thus, to avoid possible artifact in the GST pull-down assay, we used the C-terminal cysteine truncated Rab9A/9B (residues 1–199) to analyze their binding abilities with RUTBC2 RBD.

For the mutational analyses of the Rab9A-RUTBC2 RBD interaction, Rab9A Q66L (residues 1–199) was cloned into the pGEX 4T-1 plasmid (GE Healthcare) to attach a GST tag at the N terminus, and RUTBC2 RBD (residues 254–425) was cloned as above to attach a His_6 tag at the N terminus. The recombinant proteins were expressed as above. His_6-RUTBC2 RBD was purified by Ni-NTA affinity chromatography in the lysis buffer. GST-Rab9A was purified by GST affinity chromatography on glutathione-coated Sepharose beads (GE Healthcare) in the lysis buffer, as recommended by the manufacturer. Twenty micrograms (or 0.4 nmol) of GST-Rab9A were immobilized onto the glutathione Sepharose beads and then incubated with 100 μg (or 5 nmol) of His_6-RUTBC2 at 4°C for 2 hr in 1 ml lysis buffer supplemented with 1 mM GTP and 1 mM DTT. The beads were washed three times (10 min each) with the same buffer and then analyzed by SDS-PAGE with Coomassie blue staining. GST was used as control.

For the binding analyses of Rab9A/Rab9B with RUTBC1/RUTBC2, Rab9A/Rab9B Q66L with (Rab9A/Rab9B, residues 1-199) or without the C-terminal hypervariable region (Rab9AΔC/Rab9BΔC, residues 1–171) were cloned into the pET-22b plasmid to attach a His_6 tag at the C terminus, and full-length RUTBC2 (residues 1–1,093), RUTBC2 RBD (residues 254–425), and RUTBC1 RBD (residues 242–424) were cloned into the pGEX 4T-1 plasmid to attach a GST tag at the N terminus. The recombinant proteins were expressed and purified as above. GST-RUTBC1/RUTBC2 were immobilized onto the glutathione Sepharose beads and then incubated with His_6-Rab9A/Rab9B. The beads were analyzed by western blotting using anti-GST and anti-His antibodies.

using anti-GST and anti-His antibodies. GST was used as control. Rab9A/Rab9B: Rab9A/Rab9B with the C-terminal two cysteines deleted (residues 1–199); Rab9AΔC/Rab9BΔC: Rab9A/Rab9B with the C-terminal hypervariable region deleted (residues 1–171).
(B) ITC analyses of the binding affinities between Rab9A/Rab9B and RUTBC2 RBD. The dissociation constant (K_d) is indicated.
See also Figures S3 and S4.

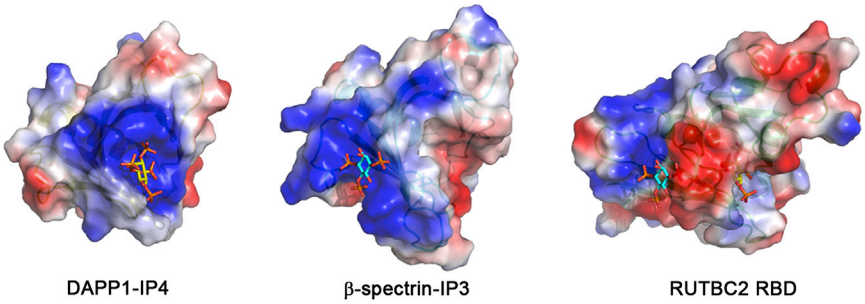

Figure 6. Comparison of the Electrostatic Surfaces of RUTBC2 RBD with DAPP1 and β-Spectrin

The three PH domain proteins are shown in the same orientation with IPs in stick models. In the DAPP1-IP4 structure (PDB code 1FAO), IP4 is bound in a positively charged pocket between the β1–β2 loop and the β3–β4 loop of the PH domain (Ferguson et al., 2000). In the β-spectrin-IP3 structure (PDB code 1BTN), IP3 is bound in a positively charged pocket between the β1–β2 loop and the β5–β6 loop (Hyvönen et al., 1995). In the RUTBC2 RBD structure, the equivalent binding sites of IP4 and IP3 in the above two complexes are indicated based on superposition of the three structures.

Isothermal Titration Calorimetry Analysis

Isothermal titration calorimetry (ITC) measurements were performed at 25°C using an ITC200 Micro-calorimeter (MicroCal). An initial injection of 0.8 μl protein sample was discarded for each data set in order to remove the effect of titrant diffusion across the syringe tip during the equilibration process. For Rab9A/Rab9B (wild-type, mutants, and variants), each experiment consisted of 20 injections of 2 μl RUTBC2 RBD (1 mM) into the sample cell containing 250 μl different Rab9 (100 μM). For RUTBC2 RBD (wild-type and mutants), the same experiments were performed with injections of 2 μl Rab9 (1 mM) into 250 μl different RUTBC2 RBD (100 μM). All the proteins were expressed and purified as described above and kept in the storage buffer. A background titration was performed using identical titrant with the buffer solution placed in the sample cell. Titration curves were fit by a nonlinear least-squares method in MicroCal Origin software version 7.0 using the single site binding model.

Immunofluorescence Microscopy Analysis

Immunofluorescence microscopy analysis was performed to analyze the colocalization of Rab9A and RUTBC2. GFP-Rab9A (residues 1–201) was cloned into the pEGFP-C3 vector (Clontech) and Myc-RUTBC2 (residues 1–1,093) into the pcDNA3 vector (Invitrogen). HeLa cells were cultured on coverslips in DMEM (Hyclone) supplemented with 10% fetal bovine serum (Biochrom), pretreated with 10 μg/ml poly-D-Lys (Sigma) for 18 hr, and then transiently transfected with the plasmids using Lipofectamine 2000 (Invitrogen). Thirty-two hours after transfection, the cells were fixed with 4% paraformaldehyde at 25°C for 15 min. Then the cells were permeabilized with 0.1% Triton X-100 in PBS for 10 min and incubated sequentially with rabbit anti-Myc antibody and the secondary antibody. The coverslips were then mounted on glass slides and the confocal images were obtained using a Leica TCS SP5 confocal microscope with a 63× oil immersion lens.

Crystallization, Diffraction Data Collection, and Structure Determination

Crystallization was performed using the hanging drop vapor diffusion method at 16°C by mixing equal volumes (1.0 μl) of protein solution (20 mg/ml) and reservoir solution. Crystals of the Rab9A-RUTBC2 complex were grown from drops containing the reservoir solution of 0.2 M ammonium acetate, 0.1 M sodium acetate (pH 5.0), and 20% (w/v) polyethylene glycol 4,000. The crystals were cryoprotected with paratone and flash-frozen in liquid nitrogen. Diffraction data were collected at −175°C at BL17U of Shanghai Synchrotron Radiation Facility and processed with HKL2000 (Otwinowski and Minor, 1997).

Structure of the Rab9A-RUTBC2 RBD complex was solved with the molecular replacement (MR) method as implemented in Phenix (Adams et al., 2010) using the GppNHp-bound Rab9A structure (Protein Data Bank [PDB] code 1YZL) (Eathiraj et al., 2005) as the search model. In the MR-phased electron density map, the structure of Rab9A was well defined, and additionally there was evident and continuous electron density for several β strands corresponding to the β1–β4 strands of RUTBC2 RBD. Iterative cycles of manual model building of a partial polyalanine model of RUTBC2 RBD and real-space refinement gradually developed more electron density that allowed us to build the full structure model of RUTBC2 RBD. Structure refinement was carried out using Phenix (Adams et al., 2010) and Refmac5 (Murshudov et al., 1997), and model building using Coot (Emsley and Cowtan, 2004). Stereochemistry of the structure model was analyzed using Procheck (Laskowski et al., 1993). Structural analyses were carried out using programs in CCP4 (Winn et al., 2011) and the PISA server (Krissinel and Henrick, 2007). Structure figures were generated using PyMOL (http://www.pymol.org). The statistics of the structure refinement and final structure model are summarized in Table 1.

ACCESSION NUMBERS

The Protein Data Bank accession number for the crystal structure of the Rab9A-RUTBC2 RBD complex reported in this paper is 4QXA.

SUPPLEMENTAL INFORMATION

Supplemental Information includes six figures and can be found with this article online at http://dx.doi.org/10.1016/j.str.2014.08.005.

AUTHOR CONTRIBUTIONS

Z.Z. performed the structure determination and some of the functional studies and drafted the manuscript. S.W. performed the cloning and protein purification experiments, the crystallization and most of the functional studies. T.S. performed the initial cloning and protein purification experiments. J.C. participated in the discussion. J.D. conceived the study, participated in the experimental design and data analyses, and wrote the manuscript.

ACKNOWLEDGMENTS

We thank the staff members at BL17U of Shanghai Synchrotron Radiation Facility, China for technical support in diffraction data collection. This work was supported by grants from the National Natural Science Foundation of China (31230017), the Strategic Priority Research Program of the Chinese Academy of Sciences (XDB08010300), and the Ministry of Science and Technology of China (2011CB966301 and 2011CB911102).

Received: March 21, 2014
Revised: August 9, 2014
Accepted: August 13, 2014
Published: September 11, 2014

REFERENCES

Adams, P.D., Afonine, P.V., Bunkóczi, G., Chen, V.B., Davis, I.W., Echols, N., Headd, J.J., Hung, L.W., Kapral, G.J., Grosse-Kunstleve, R.W., et al. (2010). PHENIX: a comprehensive Python-based system for macromolecular structure solution. Acta Crystallogr. D Biol. Crystallogr. *66*, 213–221.

Aivazian, D., Serrano, R.L., and Pfeffer, S. (2006). TIP47 is a key effector for Rab9 localization. J. Cell Biol. *173*, 917–926.

Barbero, P., Bittova, L., and Pfeffer, S.R. (2002). Visualization of Rab9-mediated vesicle transport from endosomes to the trans-Golgi in living cells. J. Cell Biol. *156*, 511–518.

 ©2014 Elsevier Ltd All rights reserved

Barr, F., and Lambright, D.G. (2010). Rab GEFs and GAPs. Curr. Opin. Cell Biol. *22*, 461–470.

Begley, M.J., Taylor, G.S., Kim, S.A., Veine, D.M., Dixon, J.E., and Stuckey, J.A. (2003). Crystal structure of a phosphoinositide phosphatase, MTMR2: insights into myotubular myopathy and Charcot-Marie-Tooth syndrome. Mol. Cell *12*, 1391–1402.

Bonifacino, J.S., and Glick, B.S. (2004). The mechanisms of vesicle budding and fusion. Cell *116*, 153–166.

Bunney, T.D., Opaleye, O., Roe, S.M., Vatter, P., Baxendale, R.W., Walliser, C., Everett, K.L., Josephs, M.B., Christow, C., Rodrigues-Lima, F., et al. (2009). Structural insights into formation of an active signaling complex between Rac and phospholipase C gamma 2. Mol. Cell *34*, 223–233.

Callebaut, I., de Gunzburg, J., Goud, B., and Mornon, J.P. (2001). RUN domains: a new family of domains involved in Ras-like GTPase signaling. Trends Biochem. Sci. *26*, 79–83.

Carroll, K.S., Hanna, J., Simon, I., Krise, J., Barbero, P., and Pfeffer, S.R. (2001). Role of Rab9 GTPase in facilitating receptor recruitment by TIP47. Science *292*, 1373–1376.

Chavas, L.M., Ihara, K., Kawasaki, M., Torii, S., Uejima, T., Kato, R., Izumi, T., and Wakatsuki, S. (2008). Elucidation of Rab27 recruitment by its effectors: structure of Rab27a bound to Exophilin4/Slp2-a. Structure *16*, 1468–1477.

Chen, L., DiGiammarino, E., Zhou, X.E., Wang, Y., Toh, D., Hodge, T.W., and Meehan, E.J. (2004). High resolution crystal structure of human Rab9 GTPase: a novel antiviral drug target. J. Biol. Chem. *279*, 40204–40208.

Chen, Z., Medina, F., Liu, M.Y., Thomas, C., Sprang, S.R., and Sternweis, P.C. (2010). Activated RhoA binds to the pleckstrin homology (PH) domain of PDZ-RhoGEF, a potential site for autoregulation. J. Biol. Chem. *285*, 21070–21081.

Díaz, E., Schimmöller, F., and Pfeffer, S.R. (1997). A novel Rab9 effector required for endosome-to-TGN transport. J. Cell Biol. *138*, 283–290.

Eathiraj, S., Pan, X., Ritacco, C., and Lambright, D.G. (2005). Structural basis of family-wide Rab GTPase recognition by rabenosyn-5. Nature *436*, 415–419.

Eathiraj, S., Mishra, A., Prekeris, R., and Lambright, D.G. (2006). Structural basis for Rab11-mediated recruitment of FIP3 to recycling endosomes. J. Mol. Biol. *364*, 121–135.

Emsley, P., and Cowtan, K. (2004). Coot: model-building tools for molecular graphics. Acta Crystallogr. D Biol. Crystallogr. *60*, 2126–2132.

Espinosa, E.J., Calero, M., Sridevi, K., and Pfeffer, S.R. (2009). RhoBTB3: a Rho GTPase-family ATPase required for endosome to Golgi transport. Cell *137*, 938–948.

Ferguson, K.M., Kavran, J.M., Sankaran, V.G., Fournier, E., Isakoff, S.J., Skolnik, E.Y., and Lemmon, M.A. (2000). Structural basis for discrimination of 3-phosphoinositides by pleckstrin homology domains. Mol. Cell *6*, 373–384.

Frische, E.W., and Zwartkruis, F.J. (2010). Rap1, a mercenary among the Ras-like GTPases. Dev. Biol. *340*, 1–9.

Fukuda, M. (2011). TBC proteins: GAPs for mammalian small GTPase Rab? Biosci. Rep. *31*, 159–168.

Ganley, I.G., Carroll, K., Bittova, L., and Pfeffer, S. (2004). Rab9 GTPase regulates late endosome size and requires effector interaction for its stability. Mol. Biol. Cell *15*, 5420–5430.

Grosshans, B.L., Ortiz, D., and Novick, P. (2006). Rabs and their effectors: achieving specificity in membrane traffic. Proc. Natl. Acad. Sci. USA *103*, 11821–11827.

Hanna, J., Carroll, K., and Pfeffer, S.R. (2002). Identification of residues in TIP47 essential for Rab9 binding. Proc. Natl. Acad. Sci. USA *99*, 7450–7454.

Holm, L., and Rosenström, P. (2010). Dali server: conservation mapping in 3D. Nucleic Acids Res. *38*, W545–W549.

Hyvönen, M., Macias, M.J., Nilges, M., Oschkinat, H., Saraste, M., and Wilmanns, M. (1995). Structure of the binding site for inositol phosphates in a PH domain. EMBO J. *14*, 4676–4685.

Itzen, A., and Goody, R.S. (2011). GTPases involved in vesicular trafficking: structures and mechanisms. Semin. Cell Dev. Biol. *22*, 48–56.

Jagoe, W.N., Lindsay, A.J., Read, R.J., McCoy, A.J., McCaffrey, M.W., and Khan, A.R. (2006). Crystal structure of rab11 in complex with rab11 family interacting protein 2. Structure *14*, 1273–1283.

Jezyk, M.R., Snyder, J.T., Gershberg, S., Worthylake, D.K., Harden, T.K., and Sondek, J. (2006). Crystal structure of Rac1 bound to its effector phospholipase C-beta2. Nat. Struct. Mol. Biol. *13*, 1135–1140.

Jin, R., Junutula, J.R., Matern, H.T., Ervin, K.E., Scheller, R.H., and Brunger, A.T. (2005). Exo84 and Sec5 are competitive regulatory Sec6/8 effectors to the RalA GTPase. EMBO J. *24*, 2064–2074.

Khan, A.R., and Ménétrey, J. (2013). Structural biology of Arf and Rab GTPases' effector recruitment and specificity. Structure *21*, 1284–1297.

Kloer, D.P., Rojas, R., Ivan, V., Moriyama, K., van Vlijmen, T., Murthy, N., Ghirlando, R., van der Sluijs, P., Hurley, J.H., and Bonifacino, J.S. (2010). Assembly of the biogenesis of lysosome-related organelles complex-3 (BLOC-3) and its interaction with Rab9. J. Biol. Chem. *285*, 7794–7804.

Krissinel, E., and Henrick, K. (2007). Inference of macromolecular assemblies from crystalline state. J. Mol. Biol. *372*, 774–797.

Kukimoto-Niino, M., Sakamoto, A., Kanno, E., Hanawa-Suetsugu, K., Terada, T., Shirouzu, M., Fukuda, M., and Yokoyama, S. (2008). Structural basis for the exclusive specificity of Slac2-a/melanophilin for the Rab27 GTPases. Structure *16*, 1478–1490.

Laskowski, R.A., Macarthur, M.W., Moss, D.S., and Thornton, J.M. (1993). Procheck—a program to check the stereochemical quality of protein structures. J. Appl. Cryst. *26*, 283–291.

Lemmon, M.A. (2004). Pleckstrin homology domains: not just for phosphoinositides. Biochem. Soc. Trans. *32*, 707–711.

Lemmon, M.A. (2007). Pleckstrin homology (PH) domains and phosphoinositides. Biochem. Soc. Symp. *74*, 81–93.

Lombardi, D., Soldati, T., Riederer, M.A., Goda, Y., Zerial, M., and Pfeffer, S.R. (1993). Rab9 functions in transport between late endosomes and the trans Golgi network. EMBO J. *12*, 677–682.

Malaby, A.W., van den Berg, B., and Lambright, D.G. (2013). Structural basis for membrane recruitment and allosteric activation of cytohesin family Arf GTPase exchange factors. Proc. Natl. Acad. Sci. USA *110*, 14213–14218.

McGourty, K., Thurston, T.L., Matthews, S.A., Pinaud, L., Mota, L.J., and Holden, D.W. (2012). Salmonella inhibits retrograde trafficking of mannose-6-phosphate receptors and lysosome function. Science *338*, 963–967.

Ménétrey, J., Perderiset, M., Cicolari, J., Dubois, T., Elkhatib, N., El Khadali, F., Franco, M., Chavrier, P., and Houdusse, A. (2007). Structural basis for ARF1-mediated recruitment of ARHGAP21 to Golgi membranes. EMBO J. *26*, 1953–1962.

Merithew, E., Hatherly, S., Dumas, J.J., Lawe, D.C., Heller-Harrison, R., and Lambright, D.G. (2001). Structural plasticity of an invariant hydrophobic triad in the switch regions of Rab GTPases is a determinant of effector recognition. J. Biol. Chem. *276*, 13982–13988.

Mishra, A., Eathiraj, S., Corvera, S., and Lambright, D.G. (2010). Structural basis for Rab GTPase recognition and endosome tethering by the C2H2 zinc finger of Early Endosomal Autoantigen 1 (EEA1). Proc. Natl. Acad. Sci. USA *107*, 10866–10871.

Murray, J.L., Mavrakis, M., McDonald, N.J., Yilla, M., Sheng, J., Bellini, W.J., Zhao, L., Le Doux, J.M., Shaw, M.W., Luo, C.C., et al. (2005). Rab9 GTPase is required for replication of human immunodeficiency virus type 1, filoviruses, and measles virus. J. Virol. *79*, 11742–11751.

Murshudov, G.N., Vagin, A.A., and Dodson, E.J. (1997). Refinement of macromolecular structures by the maximum-likelihood method. Acta Crystallogr. D Biol. Crystallogr. *53*, 240–255.

Nottingham, R.M., Ganley, I.G., Barr, F.A., Lambright, D.G., and Pfeffer, S.R. (2011). RUTBC1 protein, a Rab9A effector that activates GTP hydrolysis by Rab32 and Rab33B proteins. J. Biol. Chem. *286*, 33213–33222.

Nottingham, R.M., Pusapati, G.V., Ganley, I.G., Barr, F.A., Lambright, D.G., and Pfeffer, S.R. (2012). RUTBC2 protein, a Rab9A effector and GTPase-activating protein for Rab36. J. Biol. Chem. *287*, 22740–22748.

Ostermeier, C., and Brunger, A.T. (1999). Structural basis of Rab effector specificity: crystal structure of the small G protein Rab3A complexed with the effector domain of rabphilin-3A. Cell *96*, 363–374.

Otwinowski, Z., and Minor, W. (1997). Processing of X-ray diffraction data collected in oscillation mode. Methods Enzymol. *276*, 307–326.

Pereira-Leal, J.B., and Seabra, M.C. (2000). The mammalian Rab family of small GTPases: definition of family and subfamily sequence motifs suggests a mechanism for functional specificity in the Ras superfamily. J. Mol. Biol. *301*, 1077–1087.

Pfeffer, S.R. (2009). Multiple routes of protein transport from endosomes to the trans Golgi network. FEBS Lett. *583*, 3811–3816.

Recacha, R., Boulet, A., Jollivet, F., Monier, S., Houdusse, A., Goud, B., and Khan, A.R. (2009). Structural basis for recruitment of Rab6-interacting protein 1 to Golgi via a RUN domain. Structure *17*, 21–30.

Reddy, J.V., Burguete, A.S., Sridevi, K., Ganley, I.G., Nottingham, R.M., and Pfeffer, S.R. (2006). A functional role for the GCC185 golgin in mannose 6-phosphate receptor recycling. Mol. Biol. Cell *17*, 4353–4363.

Riederer, M.A., Soldati, T., Shapiro, A.D., Lin, J., and Pfeffer, S.R. (1994). Lysosome biogenesis requires Rab9 function and receptor recycling from endosomes to the trans-Golgi network. J. Cell Biol. *125*, 573–582.

Scheffzek, K., and Welti, S. (2012). Pleckstrin homology (PH) like domains - versatile modules in protein-protein interaction platforms. FEBS Lett. *586*, 2662–2673.

Shiba, T., Koga, H., Shin, H.W., Kawasaki, M., Kato, R., Nakayama, K., and Wakatsuki, S. (2006). Structural basis for Rab11-dependent membrane recruitment of a family of Rab11-interacting protein 3 (FIP3)/Arfophilin-1. Proc. Natl. Acad. Sci. USA *103*, 15416–15421.

Stenmark, H. (2009). Rab GTPases as coordinators of vesicle traffic. Nat. Rev. Mol. Cell Biol. *10*, 513–525.

Vetter, I.R., Nowak, C., Nishimoto, T., Kuhlmann, J., and Wittinghofer, A. (1999). Structure of a Ran-binding domain complexed with Ran bound to a GTP analogue: implications for nuclear transport. Nature *398*, 39–46.

Winn, M.D., Ballard, C.C., Cowtan, K.D., Dodson, E.J., Emsley, P., Evans, P.R., Keegan, R.M., Krissinel, E.B., Leslie, A.G., McCoy, A., et al. (2011). Overview of the CCP4 suite and current developments. Acta Crystallogr. D Biol. Crystallogr. *67*, 235–242.

Wittmann, J.G., and Rudolph, M.G. (2004). Crystal structure of Rab9 complexed to GDP reveals a dimer with an active conformation of switch II. FEBS Lett. *568*, 23–29.

Wu, M., Wang, T., Loh, E., Hong, W., and Song, H. (2005). Structural basis for recruitment of RILP by small GTPase Rab7. EMBO J. *24*, 1491–1501.

Yang, H., Sasaki, T., Minoshima, S., and Shimizu, N. (2007). Identification of three novel proteins (SGSM1, 2, 3) which modulate small G protein (RAP and RAB)-mediated signaling pathway. Genomics *90*, 249–260.

Zerial, M., and McBride, H. (2001). Rab proteins as membrane organizers. Nat. Rev. Mol. Cell Biol. *2*, 107–117.

Zhu, G., Zhai, P., Liu, J., Terzyan, S., Li, G., and Zhang, X.C. (2004). Structural basis of Rab5-Rabaptin5 interaction in endocytosis. Nat. Struct. Mol. Biol. *11*, 975–983.

 ©2014 Elsevier Ltd All rights reserved